Proceedings of the ASME 2010 3rd Joint US-European Fluids Engineering Summer Meeting and 8th International Conference on Nanochannels, Microchannels, and Minichannels
FEDSM-ICNMM2010
August 1-5, 2010, Montreal, Canada

FEDSM-ICNMM2010-31269

PARTICLE, FLUID VELOCITY, AND EROSION MEASUREMENTS FOR VISCOUS LIQUIDS IN A SUBMERGED DIRECT IMPINGEMENT FLOW

Stephen Miska stephen-miska@utulsa.edu
Siamack A. Shirazi* siamack-shirazi@utulsa.edu
Brenton S. McLaury brenton-mclaury@utulsa.edu
Yongli Zhang yongli-zhang@utulsa.edu
Edmund F. Rybicki* ed-rybicki@utulsa.edu
Risa Okita risa-okita@utulsa.edu

Department of Mechanical Engineering, The University of Tulsa

ABSTRACT

In the production and pipeline transport of various fluids, such as oil and natural gas, solid particles may be entrained in the fluid. These particles, commonly consisting of numerous types and sizes of sand, can travel apart from the streamlines of the fluid and impact the surface of the pipe. With time, enough particles may impinge a pipe wall at a sensitive location, such as an elbow or tee, to result in a measurable wall thickness loss. This may ultimately lead to severe erosion damage causing a leak in a pipeline, a dangerous and costly problem. As a result, a pipeline's service life may often depend on the rate at which a pipe wall is eroded.

The erosion rate, or amount of material loss over a certain time period, depends on a large number of factors. The target material, or material experiencing a thickness loss, such as a pipe wall, influences the rate at which damage occurs. Its density, hardness, yield strength, and microstructure combine to present a certain resistance toward erosion occurring from solid particle impact. Furthermore, the solid particle's diameter, sharpness, and shape will influence its trajectory, speed, and momentum transfer into the target, thereby requiring the analysis of various particle types in predicting erosion. Finally, the carrier fluid being transported through a pipeline will further affect the solid particle's movement as it approaches the target. As a result, the fluid's density and viscosity must be carefully considered in particle tracking and erosion analysis. By considering the aforementioned properties of the target, solid particles, and carrier fluid, it is desirable to be able to predict the erosion rate from a single erosion equation. Other factors depending on these properties may be found in this expression, such as particle impact speed and impingement angle at the target.

Velocity measurements by way of Laser Doppler Velocimetry (LDV) were made for particles entrained in a viscous liquid traveling in a submerged, direct impingement jet. In an attempt to obtain representative particle impact characteristics during material erosion, data was collected from the nozzle exit to the target surface in order to track fluid and particle velocities prior to impact with a wall. Average particle sizes of 120 and 550 μm were used to represent typical sand sizes, while much smaller particles with an average diameter of 3 μm were utilized in fluid velocity measurements. The carrier fluid viscosity was varied from 1 to 100 centiPoise, while the nozzle flow rate and fluid density were maintained constant. Changes in approach and estimated impingement velocity occurring due to fluid viscosity and particle size are then presented.

For the same impingement geometry and flow situations, metal loss erosion measurements have been made by way of an Electrical-Resistance (ER) probe. Oklahoma #1 sand particles with an average diameter of 150 μm were suspended in a viscous carrier fluid at a measured sand concentration. The measured erosion rate and particle velocities at near target wall locations are then compared to observe the effect of viscosity on material erosion and impact speed. Particle tracking and erosion predictions made by Computational Fluid Dynamics (CFD) can then be experimentally validated.

1. INTRODUCTION

1.1 Erosion Prediction Overview

In the production and pipeline transport of various fluids, such as oil and natural gas, solid particles may be

entrained in the fluid. These particles, commonly consisting of numerous types and sizes of sand, can travel apart from the streamlines of the fluid and impact the surface of the pipe. With time, enough particles may impinge a pipe wall at a sensitive location, such as an elbow or tee, to result in a measurable wall thickness loss. This may ultimately lead to severe erosion damage causing a leak in a pipeline, a dangerous and costly problem.

The erosion rate, or amount of material loss over a certain time period, depends on a large number of factors. Among these variables are the entrained particle's diameter, sharpness, and shape, all of which will influence a solid particle's trajectory, speed, and momentum transfer into the target. This consequently requires the analysis of various particle types in predicting erosion. The carrier fluid being transported through a pipeline will further affect the solid particle's movement as it approaches the target. As a result, the fluid's density and viscosity must be carefully considered in particle tracking and erosion analysis. By considering the aforementioned properties of the entrained solid particles and carrier fluid, it is desirable to be able to predict the erosion rate from a single erosion equation which takes into account particle impact speed and impingement angle at the target.

An experimental study of erosion may be performed by measuring actual target material losses over time for a given geometry and flow situation. In addition, particle tracking, or measuring a particle's velocity, angle, and location as it approaches and impinges a target, is also possible by experiment. At the same time, computational fluid dynamics (CFD) can use transport phenomena theory and computer-based numerical techniques to predict the particle trajectory, including particle impact velocity, for many geometries and flow cases. By incorporating current erosion equations based on empirical testing, CFD can then also provide erosion predictions for the geometry of interest.

1.2 Research Goals and Approach

Previous research work has been directed at improving an erosion ratio equation by way of a combination of experimental and computational work. More specifically, the direct jet impingement of solid particles released from a fluid submerged nozzle has been carefully studied. Such a flow situation allows for solid particles to travel through a carrier fluid moving with a controlled flow rate prior to being released through a nozzle. At the nozzle exit, solid particles will travel through a certain length prior to impacting a target. When properly studied and evaluated, this flow scenario can be related to erosion in another common geometry, such as a pipe elbow or tee.

The research to be discussed involves measuring the effect of the carrier fluid viscosity on solid particle tracking and erosion rate for the direct impingement geometry to be described. Particle velocities, including near wall velocities, have been measured and can be compared to CFD predictions. Different fluid viscosities were used and Laser Doppler Velocimetry (LDV) was utilized to measure particle and fluid speeds. The velocity of particles near the wall is examined for different carrier fluids in order to explain erosion rates that occur as a result of particle impact.

2. LITERATURE REVIEW AND BACKGROUND

Erosion resulting from solid particle impact on a material has been studied by numerous researchers using various experimental, computational, and theory-driven techniques.

Meng and Ludema (1995) investigated various erosion models and equations which have been used to make erosion predictions in the past [1]. A conclusion from this research indicated that a single comprehensive model cannot be practically established for general use due to the complexity of the factors influencing erosion. Since over one hundred various parameters and factors have been suggested to affect material erosion and many different erosion mechanisms have been proposed, a single model explicitly using all necessary factors and variables has yet to be produced. Common factors, however, such as particle velocity, particle size, particle shape, target material hardness, target yield strength, carrier flow velocity, carrier fluid density, and carrier fluid viscosity, have consistently been cited as key variables dictating erosion.

Bitter (1963) suggested that erosion occurred simultaneously by two separate material wear mechanisms [2]. These included deformation wear, which occurs due to material cracking instigated by the normal velocity component of impinging particles, and cutting wear, which occurs when particles impact at angles parallel to the surface, thus causing scraping of the material. It was further proposed that erosion occurs as a sum of these two wear mechanisms, thus requiring separate equations to predict deformation erosion and cutting erosion. This called for the need to track particles in two mutually-normal directions.

Clark (1992) suggested that experimental data on erosion rates for a given material can be predicted only if representative particle impact velocities and trajectories are known [3]. Liquid viscosity and density, as well as particle impingement velocity, angle of impact, and size range, were listed as key variables in laboratory testing. It was further concluded that forces acting on a particle close to a target surface must be further investigated by way of using analytical models of particle trajectories combined with experimental erosion test methods.

Earlier, Clark (1991) performed experiments to measure the impact rate and energy of particles in a slurry pot erosion tester [4]. For these tests, erosion was estimated by the size of impact craters caused by glass bead particles on a copper rod target for a water-glycerin carrier fluid of varying viscosity. Using this method, the calculated particle impact speed decreased significantly with increasing carrier liquid viscosity. It was found that increasing viscosity and decreasing particle size resulted in a reduction in erosion rates due to the flow interaction of the fluid, particles, and eroding surface.

Wong (1993) presented an analytical model to quantitatively describe particle trajectories and impact velocities on a cylindrical erosion target [5]. This model considered effects influenced by the carrier fluid properties, such as drag, inertia and pressure variation acting on a particle approaching the target surface. When compared to experimental data gathered by Clark (1991), the effects of change of liquid viscosity and particle size were predicted accurately by the model [4]. At the same time, the model predicted the formation of a sliding bed of particles along the target surface for lower impact velocities, thus suggesting the potential for erosion caused by abrasion or deformation wear.

Laser-Doppler Velocimetry (LDV) has successfully been used in past experimental studies to measure fluid and particle velocities. Barata (2004) used LDV to measure the flow field resulting from the direct impingement of an axisymmetric jet on a solid target after encountering a confined cross flow [6]. During this research, particles as small as 1-4 μm were used to accurately measure fluid flow in turbulent gas jets. Sasaki (1980) used LDV to measure the falling velocity and size of large rain droplets ranging in size from 0.1 to 1.0 mm [7]. Ancimer (1999) presented LDV measurements of seeded particles in a spark ignition engine and was able to obtain valid velocity measurements with sufficient frequency shifts and high data rates [9].

3. EXPERIMENTAL FACILITY

3.1 General Description of Experimental Facilities

Two experimental facilities have been constructed to measure solid particle velocities and erosion rates. Both facilities are flow loops designed to re-circulate a liquid of variable viscosity at or below 8.0 gallons per minute, resulting in a maximum fluid velocity of approximately 10.5 m/s. Particles can be readily added and suspended in the liquid, which is pumped at the desired flow rate through a nozzle positioned directly at a target. Nozzle inner diameters in both facilities are 8 mm or 5/16 inch. For all tests, the nozzle exit is submerged in the liquid and located 12.7 mm or 0.5 inch away from the solid target. This distance serves as the stagnation length during which particle tracking can be observed. One flow loop is used primarily for particle velocity measurements with Laser Doppler Velocimetry (LDV). The other experimental facility is utilized for erosion rate or metal loss measurements with an electrical-resistance (ER) probe. Preliminary erosion measurements were performed by Okita (2008) using this flow loop. These two experiments will ultimately make it possible to relate particle impact speed to erosion rate for various fluid viscosities and particle sizes used in the facilities.

3.2 Flow Loop for Laser Doppler Velocimeter Measurements

In order to obtain solid particle velocity measurements using Laser Doppler Velocimetry (LDV), a flow loop such as the one seen in the schematic of Figure 1 was constructed.

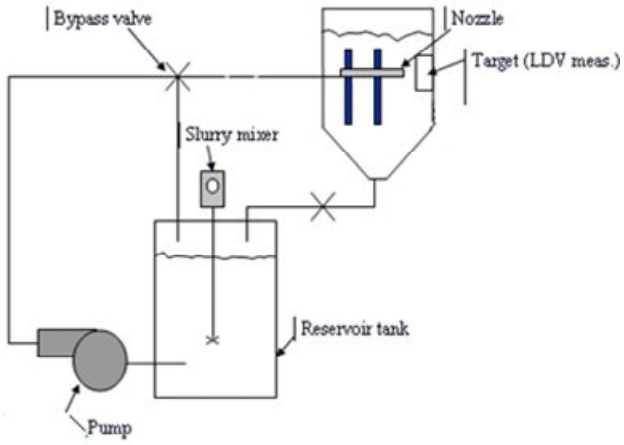

Figure 1: Flow Loop Schematic for LDV Measurements

The entire system is filled with at least 70-75 liters of a fluid having a desired viscosity achieved by mixing appropriate amounts of water and glycerin. The upper tank (or testing tank) contains around 45 liters of the liquid so as to maintain a liquid level which ensures a submerged jet at the nozzle exit. This testing tank is made of transparent acrylic so LDV measurements may be taken between the nozzle exit and the solid target. About 50 grams of highly reflective aluminum particles with an average diameter of 3, 120, or 550 μm are added to the liquid in the reservoir tank and suspended in the fluid by way of a slurry mixer. These particles have a density of approximately 2,650 kg/m^3 (about the same as the density of OK #1 sand commonly used in industry). The particle-liquid mixture is pumped through a Hydra-cell Pump and past a bypass valve which controls the velocity at the submerged nozzle exit located in the acrylic tank. Regardless of the fluid viscosity or particle diameter, the pump always displaces a flow rate of about 8.0 gallons per minute.

Local solid particle velocity measurements with the LDV were made at several different locations at and away from the nozzle centerline and exit. For the exact measurement locations, refer to Figure 2 below. Note that z = 0 mm refers to the nozzle centerline, while z = 4 mm refers to the distance at the OD of the nozzle, and z = 12 mm is 12 mm away from the centerline. In addition, the target is located at a distance of 12.7 mm from the nozzle exit. It is also necessary to observe that due to the geometry of the facility and LDV probe which emits laser beams, the closest near-wall axial velocity measurements can be made 0.6 to 0.7 mm from the target. On the other hand, it is possible to make radial velocity measurements as close as 0.1 mm from the target wall.

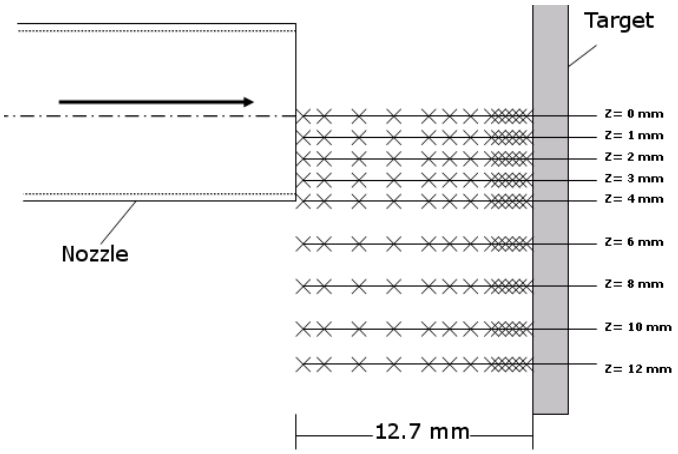

Figure 2: LDV Measurement Locations Relative to Submerged Nozzle

3.2 Flow Loop for Erosion Rate Measurements

A separate flow loop was constructed to measure the erosion rate resulting from direct impingement of a submerged jet in the same geometry as the one used in the LDV flow loop. Once again, the distance between the nozzle exit and the target is 12.7 mm. Sand is mixed with liquid prior to the experiments so that the mixture of solid particles and fluid is constantly stirred by the mixer. This prevents excess sand from sinking to the bottom of the tank and constraining the pump inlet. Recall that the straight nozzle (normal to the target) is completely submerged in the liquid. As in the LDV flow loop, the nozzle inner diameter is about 8 mm. The nozzle exit velocity of the mixture can be controlled by changing the frequency of a variable speed motor driving a pump

Two different sand particles were used for experiments with this flow loop: Oklahoma #1 sand with an average size of 150 microns and California 60 mesh sand with an average particle size of 300 microns. The density of both sands is about 2,650 kg/m^3 (similar to the density of the aluminum particles used in LDV measurements). From sand size distribution measurements for OK #1 sand, it is seen that although the average size is about 150 μm, some sand particles may be as small as 80 μm or as large as 350 μm.

In order to vary the viscosity of the liquid, either CMC (Carboxymethyl Cellulose) or glycerin was mixed in with water. Since both CMC-water and glycerin-water mixtures have densities similar to that of water, viscosity was increased without significantly changing the density of the carrier fluid. Recall that glycerin was used to make the carrier fluid in the LDV tests since the glycerin solution possesses a more transparent appearance and allows LDV beams to penetrate through the mixture and accurately make particle velocity measurements. At the same time, glycerin's costliness makes it an unpractical fluid to be used in erosion testing where the appearance of the fluid is irrelevant. In order to run numerous experiments efficiently and economically, the use of CMC for erosion measurement experiments was necessary. It is important to note that CMC is made of long chain polymers which when mixed with water might act as a non-Newtonian fluid (for higher viscosities) whereas the glycerin solution is a Newtonian fluid. Tests were performed to investigate the similarity of a mixture made with CMC dissolved in water and a mixture consisting of water and glycerin. Erosion measurements were made for viscosities ranging from 1 to 50 CP.

4. EXPERIMENTAL FLUID AND PARTICLE VELOCITY RESULTS

4.1 Introduction

Axial and radial velocities of solid aluminum particles traveling from a submerged nozzle normally directed toward a target, as seen in the test setup displayed in Figure 1, were recorded with Laser Doppler Velocimetry at the locations seen in Figure 2. Consequently, particle speeds and trajectories were measured as they exited the nozzle and approached the solid wall. While the fluid flow rate was held at a constant 8.0 gallons per minute, the fluid viscosities used were 1, 10, 25, 50 and 100 CP for three particle sizes of 3, 120, and 550 microns. The data will be presented in the following manner:

a.) With particle size held constant at 3 microns in order to investigate the effect of viscosity on flow in this geometry

b.) With viscosity held constant at 100 CP in order to show the effect of particle size in a laminar flow situation

c.) With viscosity held constant at 1 CP in order to display the effect of particle size in a turbulent flow situation

The measured data, axial and radial velocities, are then used to construct speed contours based on the magnitude of the measured velocities at all of the locations of Figure 2.

4.2 LDV Results

4.2a Particle Size Constant at 3 microns - Effect of Viscosity on Flow

When aluminum particles with an average diameter of 3 μm are seeded in the carrier fluid, minimal to no-slip between the particles and the fluid can be assumed. At the same time, viscosities are varied to observe the change in particle and fluid trajectory as flow approaches the solid-wall target. Table 1 below shows the estimated Reynolds number for pipe flow through the nozzle. Since diameter, approximate fluid density, and average nozzle exit speed (flow rate) are held constant, viscosity is the only variable causing the change in Reynolds number.

Table 1: Reynolds Numbers of Flow with Variable Viscosity

Fluid Viscosity (CP)	Reynolds Number (Re_D)	Flow Regime (Pipe)
1	85,000	Fully turbulent
10	8,500	Fully turbulent
25	3,400	Transitional/ Turbulent
50	1,700	Transitional to laminar
100	850	Fully Laminar

These values for Reynolds Number were approximated by using Equation 1 below, where D is the nozzle diameter, ρ is the fluid density (about 1,000 kg/m^3), V is the average fluid velocity through the nozzle, and μ is the dynamic viscosity.

$$\mathrm{Re}_D = \rho VD/\mu \qquad (1)$$

Figure 3 seen below shows the axial velocity profile generated from LDV measurements at 1 mm from the nozzle exit. Typical pipe flow is observed within the 8 mm nozzle diameter. Again, note that the flow rate is held constant at 8.0 gallons per minute even as fluid viscosity is altered. Integrating each of the curves of Figure 3 over the cross-sectional area of the nozzle will yield an approximate flow rate of 8.0 GPM for each case. Furthermore, the average velocity of each curve results in a value of about 10.5 m/s.

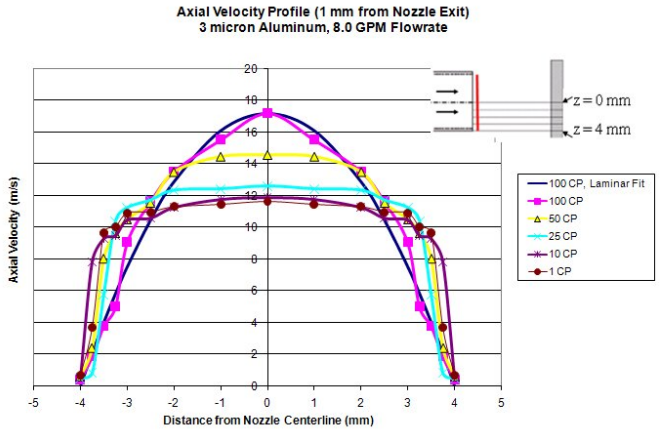

Figure 3: Axial Velocity Profile near Nozzle Exit for 3 μm Particles

It is clear that the flow predictions based on calculated Reynolds number seen in Table 1 are accurately displayed in the velocity profiles of Figure 3. The 100 CP viscosity case evidently possesses a laminar velocity profile which matches a theoretical laminar curve fit based on flow within a pipe. As expected, the 50 CP and 25 CP cases begin to show a transition from laminar to turbulent flow. The lower viscosity cases of 10 CP and 1 CP exemplify typical turbulent flow as seen in the constant axial velocity profiles followed by a sudden drop at the nozzle diameter caused due to wall shear stress.

The change in the axial velocity component (direction parallel to nozzle wall) versus distance from the nozzle exit along the nozzle centerline (defined as z=0 mm) is seen in Figure 4. Recall that the target is located 12.7 mm from the nozzle exit and the final axial velocity measurement with LDV can be made approximately 0.6 mm from the wall due to limitations imposed by the target geometry. In Figure 4-2 it is seen that the axial velocity is retained or held constant for each viscosity case until the particles travel about 8 mm from the nozzle exit. At this point, there is sudden drop in axial velocity with an apparent drop to nearly zero at the wall (the last axial velocity measurements are below 2 m/s).

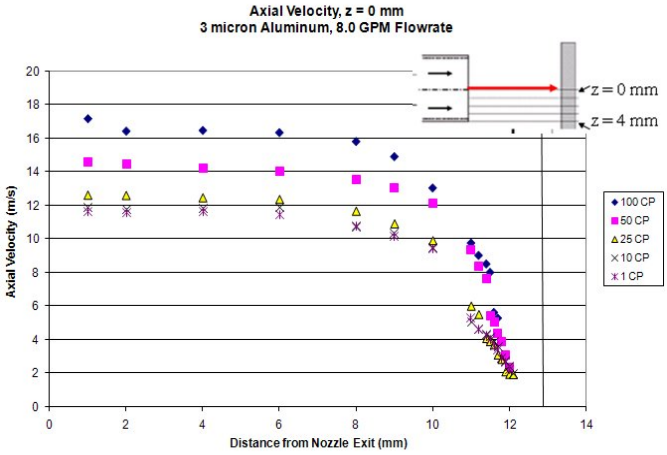

Figure 4: Axial Velocity versus Distance from Nozzle Exit at z=0 mm for 3 μm Particles

It is furthermore displayed that the higher viscosity cases of 100 CP and 50 CP possess higher initial axial velocities at the centerline due to the laminar flow transition. The lower viscosities of 25, 10, and 1 CP (which are closer to turbulent flow) possess very similar initial axial velocities. Ultimately, however, it appears that the axial velocity at the wall decays to below 2 m/s for all of the viscosity cases at this location.

Figure 5 shows the change in axial velocity versus distance from the nozzle exit for a radial distance away from the nozzle centerline of z = 3 mm. It is again seen that velocities are constant until 8 mm from the nozzle exit at which point values rapidly drop to below 2 m/s by the time particles reach the wall. Furthermore, initial velocities for all viscosity cases become more similar away from the centerline due to wall shear stress effects.

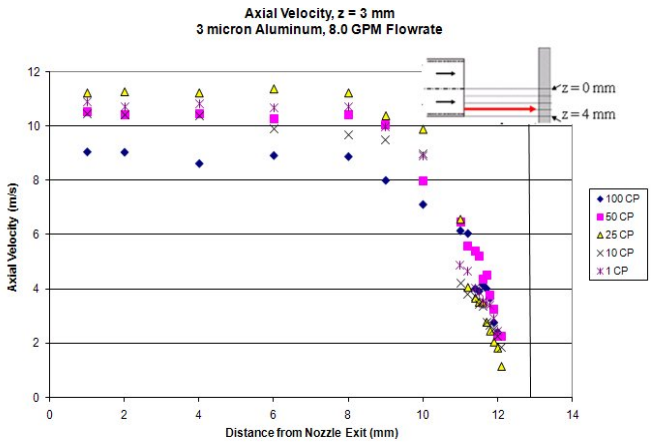

Figure 5: Axial Velocity versus Distance from Nozzle Exit at z=3 mm for 3 µm Particles

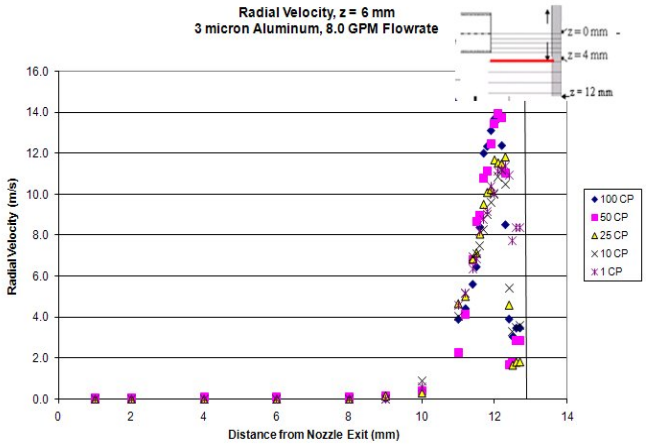

Figure 6: Radial Velocity versus Distance from Nozzle Exit at z=6 mm for 3 µm Particles

At the same time, the radial velocity component, which travels parallel to the target wall, was recorded for the same radial distances (z = 0 to 12 mm). This velocity component reaches a maximum value in the 6-8 mm radial region, with increasing viscosity normally resulting in higher maximum radial velocity values. As seen in Figure 6, which shows the radial velocity versus distance from the nozzle exit at 6 mm from the centerline (this component is negligible at the centerline), the radial velocity component does not become apparent until approximately 8 mm from the nozzle exit, at which point there is a significant increase in its magnitude. A peak in this component occurs about 1 mm from the wall which is then followed by a sudden drop at the wall for the 10, 25, 50 and 100 CP viscosity cases. The 1 CP case does not display this sudden drop at the wall. At the same time, the radial velocity peak values seen at 1 mm from the wall increase with increasing viscosity. This is most likely attributed to the higher initial axial velocities occurring near the centerline for the more viscous cases due to the turbulent to laminar transition evidenced in Figure 3. These axial velocities are transferred to radial velocities as particles tend to move outward away from the nozzle exit and closer towards the solid wall.

It is clear from near-wall LDV measurements that radial velocity undergoes significant changes in magnitude in the last 1 mm to the wall. However, it is more difficult to observe the effect of viscosity on the radial velocity at certain fixed distances from the wall. Figure 7 displays the radial velocity as a function of radial distance from the nozzle centerline (z) at a fixed distance of 0.3 mm from the wall. This is where the closest accurate radial velocity measurements could be made with LDV, most likely because the thickness of the control volume (volume of measurement) is slightly more than 0.2 mm. Further note that these measurements were taken at a distance from the peak in velocity observed in Figure 7. It is evident that the peak in radial velocity occurs between 4-8 mm for all viscosity cases. Furthermore, the radial velocity is clearly and consistently highest for the 1 CP fluid at this near wall location. For the more viscous cases of 10, 25, 50, and 100 CP, radial velocity appears to increase slowly with increasing viscosity. However, all of these values are still significantly less than one-half the radial velocities measured for the particles seeded in the 1 CP case.

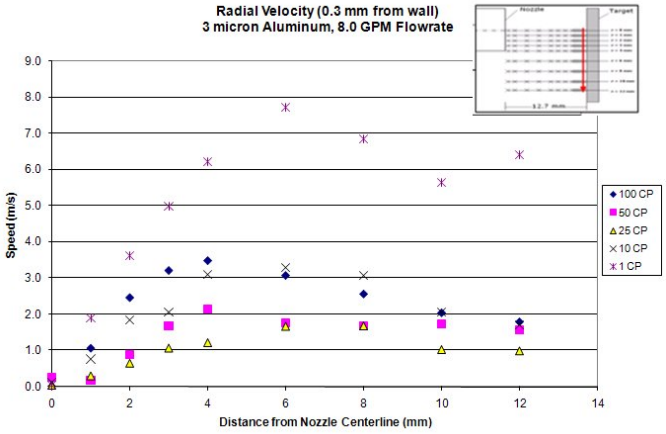

Figure 7: Radial Velocity versus Distance from Nozzle Centerline at 0.3 mm from Wall for 3 µm Particles

Figure 8 again shows the radial velocity versus radial distance from the nozzle centerline. However, these values were measured at a fixed distance of 0.6 mm from the wall, or the approximate location of the peak observed in Figure 6. Again, it is evident that the maximum radial velocity occurs 4 to 8 mm from the centerline and outside of the nozzle diameter. It is immediately evident that the velocity values increased significantly from those recorded at 0.3 mm closer to the wall (by as much as 4 times or more) for the viscous fluids of 10, 25, 50, and 100 CP. The water case of 1 CP appears to have mostly unchanged velocity values between 0.3 mm and 0.6 mm from the wall. At the same time, an increase in viscosity appears to usually increase the radial velocity at this location. This most likely occurs due to the increased axial velocities at the nozzle exit which occur as a result of the laminar transition previously addressed. However, there is the notable exception of the 100 CP case possessing the lowest radial velocities outside of the nozzle diameter of z=4 mm. Once above a given viscosity, the fluid or seeded particles may struggle to retain radial velocities as the fluid is pushed further outward and away from the nozzle exit. Within the nozzle diameter, the radial velocities continue to increase with increasing viscosity.

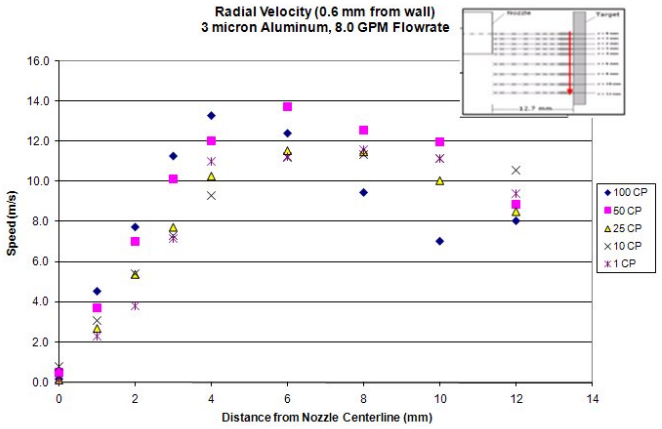

Figure 8: Radial Velocity versus Distance from Nozzle Centerline at 0.6 mm from Wall for 3 µm Particles

In order to better display the change in radial velocities in the near wall region, this measured value is plotted versus distance from the nozzle centerline at a set radial distance with a focus on the 1 mm region closest to the wall. Figure 9 shows this plot at a distance of 3 mm from the centerline, while Figure 10 contains the plot at a radial distance of 10 mm. It is important to note that the final two data points closest to the wall for each of these graphs lie inside of the 0.3 mm accurate measurement region and were not fully used in further analysis. Nevertheless, it is clear that for the viscous cases there is a significant drop in radial velocity between 0.6 mm and 0.4 mm from the wall. A much less apparent drop occurs for the non-viscous 1 CP water case. This may imply that a boundary layer approximately 0.5 mm thick forms as a result of increased viscosity for the 10, 25, 50, and 100 CP carrier fluids. At the same time, this may suggest post-impact speeds are being measured at the near-wall regions, thus resulting in the significant velocity readings. If this were true, then particles in the 1 CP fluid make lesser contact or have less of a momentum transfer as they make contact with the wall. Recall these results are for very small particles with minimal velocity slip between it and the fluid. Larger particle sizes closer to typical sand will be investigated in upcoming sections.

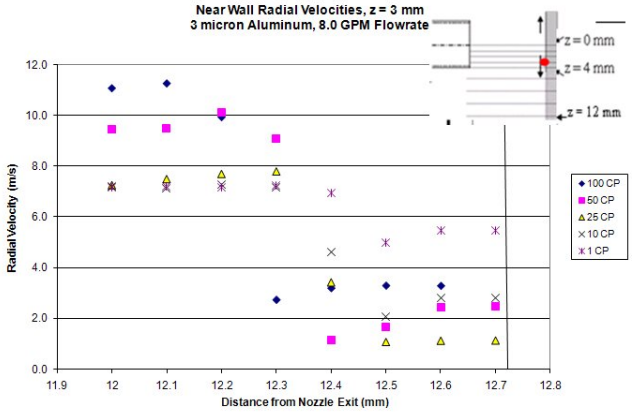

Figure 9: Near Wall Radial Velocities at z=3 mm for 3 µm Particles

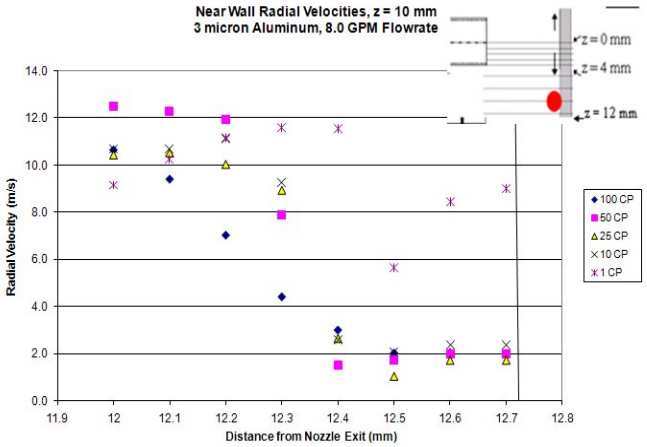

Figure 10: Near Wall Radial Velocities at z=10 mm for 3 µm Particles

In order to better visualize the axial and radial velocity measurements made by LDV in the numerous locations of the testing region, contour plots such as those seen in Figures 11 and 12 were created. Figure 11, which uses data from the 100 CP case, clearly shows the high axial velocities within the nozzle exit region and the decrease in this velocity component as measurements were made closer to the wall. The laminar velocity profile close to the nozzle exit (on the far left-hand side of the contour) is also clearly visible. At the same time, Figure 12, which is also based on the 100 CP viscosity fluid, displays the radial velocities recorded in the testing region. The rapid increase and then near-wall

decrease in radial velocities are evidently seen outside of the nozzle diameter and near to the solid wall target.

The speed of the seeded particles at any measurement location can be easily calculated by finding the magnitude of the axial and radial velocity components. Speed contours for the highest and lowest tested viscosities are seen below in Figures 13 and 14. These contours show the movement of seeded particles as they emerge from the nozzle exit with a high axial velocity which is then converted to a large radial velocity along the wall and outward from the nozzle centerline.

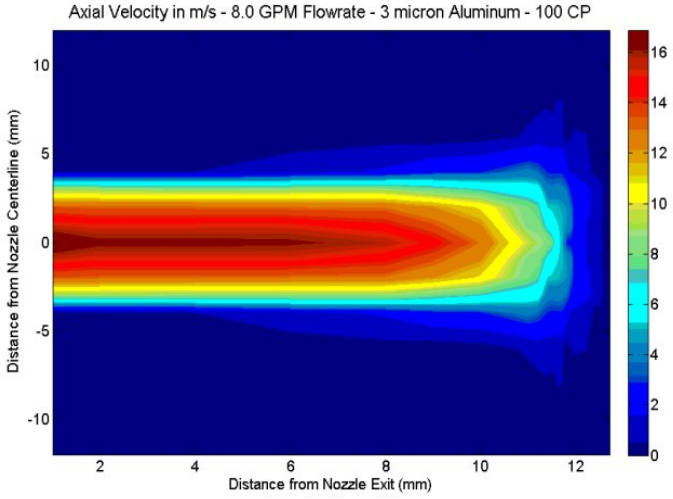

Figure 11: Axial Velocity Contour in m/s at Fluid Viscosity = 100 CP for 3 µm Particles

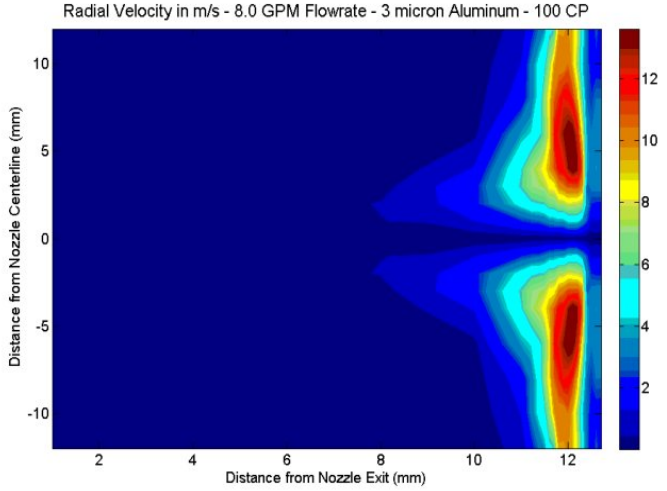

Figure 12: Radial Velocity Contour in m/s at Fluid Viscosity = 100 CP for 3 µm Particles

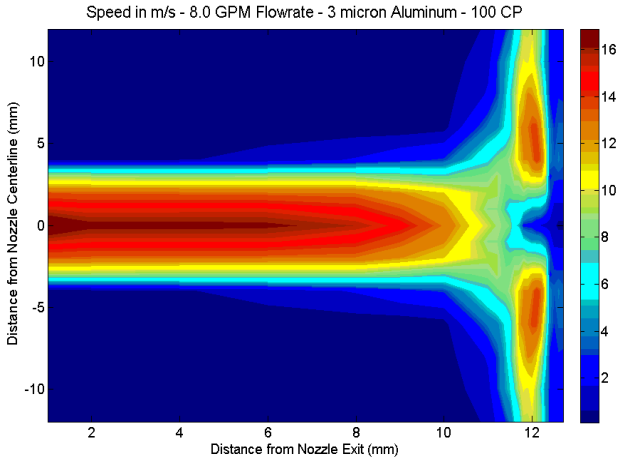

Figure 13: Speed Contour in m/s at Fluid Viscosity = 100 CP for 3 µm Particles

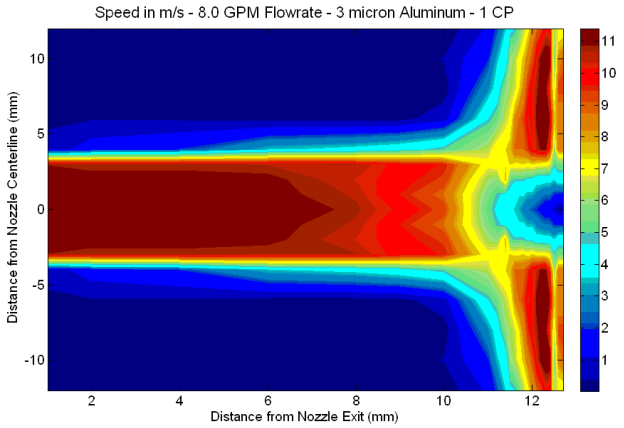

Figure 14: Speed Contour in m/s at Fluid Viscosity = 1 CP for 3 µm Particles

4.2b Fluid Viscosity Constant at 100 CP - Effect of Particle Size in Laminar Flow

LDV particle velocity measurements which have been presented thus far were shown such that average seed particle size was maintained and viscosity was altered from 1 to 100 CP. Since three particle sizes of 3, 120, and 550 microns were used, these results can also be presented for a constant fluid viscosity so that any slip or discrepancy between particle velocities may be properly investigated.

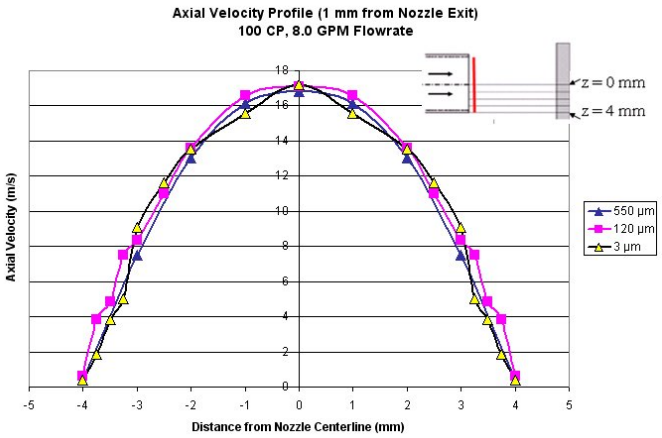

Figure 15: Axial Velocity Profile near Nozzle Exit for 100 CP Fluid

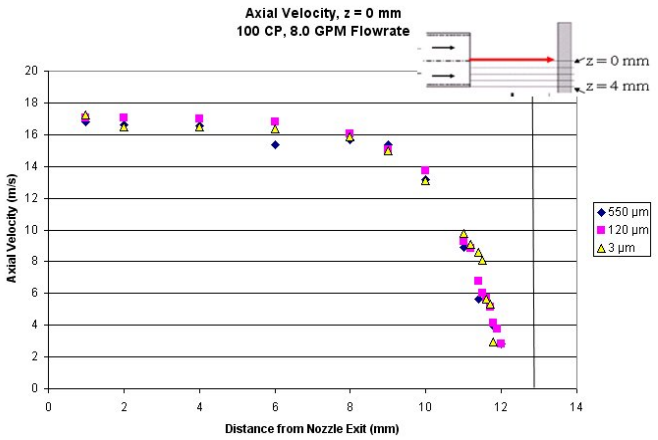

Figure 16: Axial Velocity versus Distance from Nozzle Exit at z=0 mm for 100 CP Fluid

The above plot seen in Figure 15 shows axial velocity measurements taken with LDV at 1 mm from the nozzle exit for a carrier fluid with a viscosity of 100 CP. Three separate tests were performed with seeded particles having average sizes of 3 microns, 120 microns, and 550 microns. Note that once again the fluid flow rate through the submerged nozzle was held at a constant of 8.0 gallons per minute for all experiments.

For this viscosity case, the estimated Reynolds number of 850 corresponds to fully laminar flow through the nozzle. It is clear that the experimental velocity curves seen in Figure 15 exhibit all the properties of a laminar profile for all three particle sizes. No significant slip is present between any particle size at any point on this curve. It therefore appears that at the nozzle exit, the largest particles still retain the approximate velocity of the fluid.

Axial velocities for incremental distances from the nozzle exit were also recorded to observe any changes as the exiting jet flow approached the solid wall. Figure 16 below shows these results along the nozzle centerline, defined as z=0 mm. Once again, all three particle velocities share nearly the same profile as flow approaches the target. In other words, no significant axial slip occurs along the centerline for the 100 CP fluid.

As seen in previous plots of this sort, particles begin to decelerate from their initial velocity around 8 mm from the nozzle exit. At this point, there is a significant velocity drop until the final axial measurement about 0.6-0.7 mm from the target. By the time flow reaches this location, measured particle velocities are about 2 m/s for all three particle sizes. This is a drastic reduction from the initial nozzle exit velocity of about 17 m/s and may imply near-zero axial velocities at impingement.

The axial velocity profile from the nozzle exit to the target at 3 mm from the centerline is shown in Figure 17. Similar trends as those observed in previous such plots are seen, but lower initial velocities are recorded as the nozzle wall region is approached and wall shear stresses begin to affect the laminar flow. Furthermore, there is much more disparity between the different particle size measurements, seen most at 3 mm from the centerline or in Figure 17. It appears that the largest particles possess the lowest initial axial velocities along these lines of measurement. However, the trend is retained for all particle sizes and the nearest target wall velocities appear to drop below 2 m/s for all cases.

It is important to note that this may indicate some slip between the large 550 micron particles and the fluid in the near nozzle wall region. At the same time, it is possible that increased turbulence may occur closer to the nozzle wall (at z=2 to 4 mm), thus resulting in a greater disparity between measured velocities. Overall, it seems that for the viscous 100 CP fluid, axial velocities are largely retained inside the nozzle diameter for all locations between the nozzle and the target, regardless of particle size seeded in the fluid.

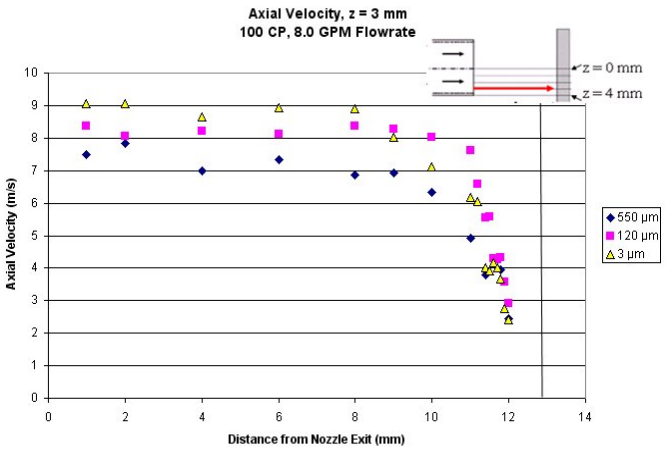

Figure 17: Axial Velocity versus Distance from Nozzle Exit at z=3 mm for 100 CP Fluid

The radial velocity component, which is parallel to the target wall and thus normal to the nozzle exit plane, was measured alongside the axial particle velocities with LDV. Figure 18 below displays the measured radial velocities for particles in the 100 CP fluid from the nozzle exit to the target wall at 6 mm from the centerline. As seen in previous such plots, the radial velocity component becomes non-zero around 8-10 mm from the centerline and rises sharply to a peak within 1 mm to the target wall. As is the case for the most viscous fluid, this peak is followed by a sharp decline in radial velocity by the last radial velocity measurement location about 0.2 to 0.3 mm from the wall, thus possibly evidencing a boundary layer effect.

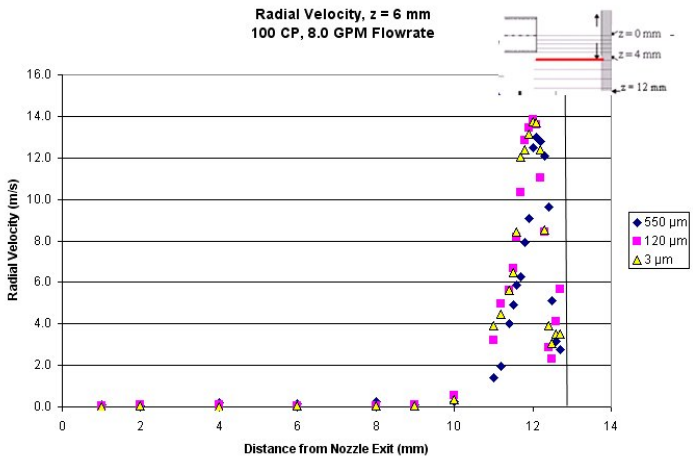

Figure 4-18: Radial Velocity versus Distance from Nozzle Exit at z=6 mm for 100 CP Fluid

These results again indicate little to no variation in measured velocity between the three different particle sizes. A large radial velocity slip is not visible in these plots between the largest and smallest particles. Trends appear to be consistent and the magnitudes of the peak values seem to be approximately the same for all particle sizes tested. There is, however, some discrepancy in the near target wall region, or in the final 1 mm to the wall.

Radial velocity measurements at a constant 0.3 mm from the wall for all three particle sizes in the 100 CP fluid are displayed below in Figure 19. The distance from the centerline is varied from 0 to 12 mm for this plot. Note that this is the location of the last accurate radial velocity measurement with LDV and is most representative of impingement speed at the wall since axial velocities are minimal along this line.

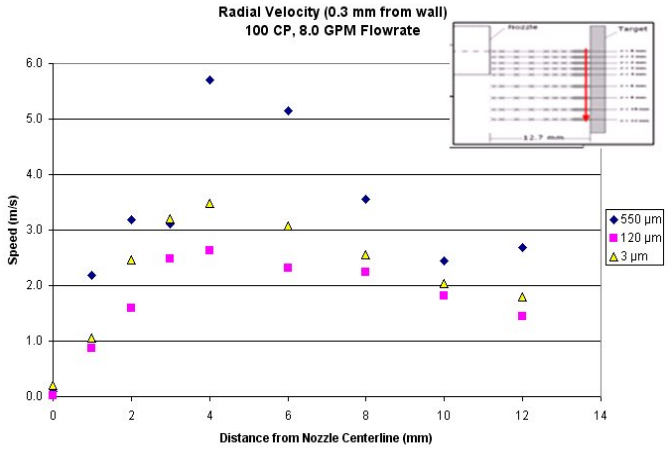

Figure 19: Radial Velocity versus Distance from Nozzle Centerline at 0.3 mm from Wall for 100 CP Fluid

It is clear that radial velocities are relatively low for the most part here when compared to the peak velocity of nearly 14 m/s. Also, it is seen that the peak in radial velocity still occurs around 4-8 mm from the centerline. Furthermore, significant variation in measured radial velocity is visible between the largest and smallest particles. The 550 micron particles consistently possess a higher velocity than the 3 and 120 micron particles. It appears that the two smaller sizes have comparable velocities with almost no slip. This may indicate that the slip in the large particle occurs due to increased momentum allowing for its radial velocity to be maintained at this extreme near wall location. Since a similar slip is not seen between the 120 and 3 micron particles, this may suggest a certain momentum threshold is necessary for velocity variance between the fluid and particle at a near-wall location.

The same type of radial velocity results are plotted at an additional 0.3 mm from the wall in Figure 20. It is clear that this line of measurement is much nearer to the peak observed in the previous figures, as evidenced by the maximum velocity exceeding 13 m/s. Again, the highest radial velocity values are obtained between 4-8 mm from the nozzle centerline.

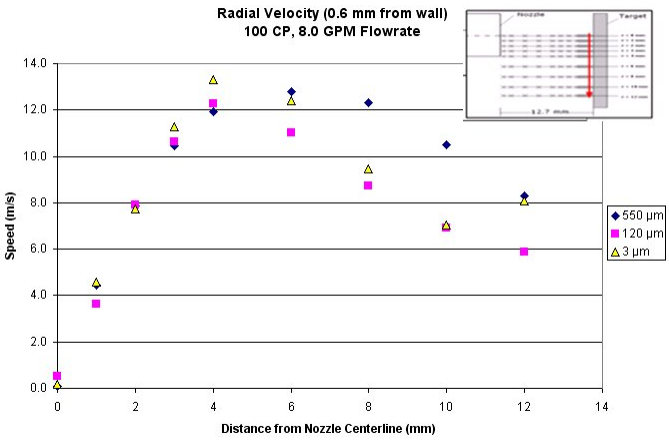

Figure 20: Radial Velocity versus Distance from Nozzle Centerline at 0.6 mm from Wall for 100 CP Fluid

As was the case at 0.3 mm from the wall, there is little to no slip between the 120 and 3 micron particles for all distances from the centerline. On the other hand, the 550 micron particles possess nearly the same velocity inside the nozzle diameter but proceed to maintain a higher velocity than the smaller particles at distances greater than 4 mm from the centerline. This slip may again imply that the 550 microns possess sufficient momentum to maintain higher velocities away from the nozzle exit and toward the solid target.

It is clear that there is a significant difference in the radial velocity values measured in Figures 19 and 20. Namely, there is drastic reduction in particle velocity between 0.6 and 0.3 mm form the wall. This may imply the formation of a boundary layer or some other interference caused by the target. This near wall region is examined further in the plots on the following pages to demonstrate the effect of particle size in this region.

Figure 21 shows these near wall radial velocities in the final 0.7-0.8 mm to the target wall at 3 mm from the centerline. High initial velocities are seen due to the peak observed in Figure 18. A significant reduction in velocity, nearly 80 percent, is observed around 0.4-0.5 mm from the wall. This may provide the thickness of the boundary layer at this location for the 100 CP fluid.

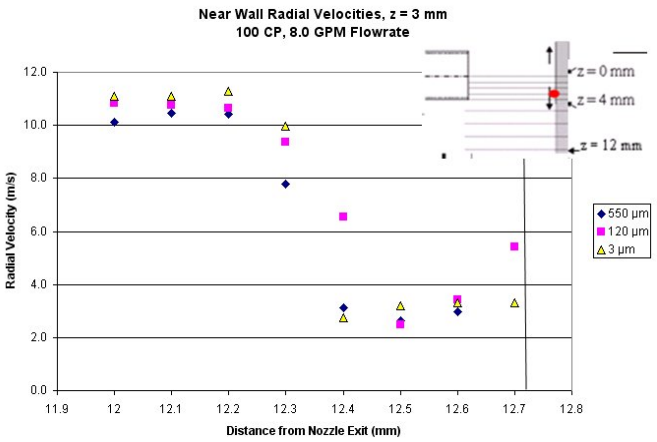

Figure 21: Near Wall Radial Velocities at z=3 mm for 100 CP Fluid

As seen in Figure 21, little to no discrepancy in velocity is evident for the three particle sizes. In other words, there is no visible slip between the largest tested particles and the viscous carrier fluid. Since these measurements were made within the inner nozzle diameter region, it is possible that the increased momentum of the 550 microns has yet to cause a visible effect in terms of an increased velocity.

Figure 22, contains a similar plot, but located 10 mm from the nozzle centerline. High initial velocities are seen again followed by an 80% reduction by the last accurate measurement which is 0.2-0.3 mm from the target. It appears that the boundary layer thickness has increased by about 0.2 mm from that seen in Figure 21. This may occur since the viscous flow develops more in the radial direction as the distance from the centerline has increased. Other interference from the wall may also be more significant at radial distances further away from the axially impinging jet.

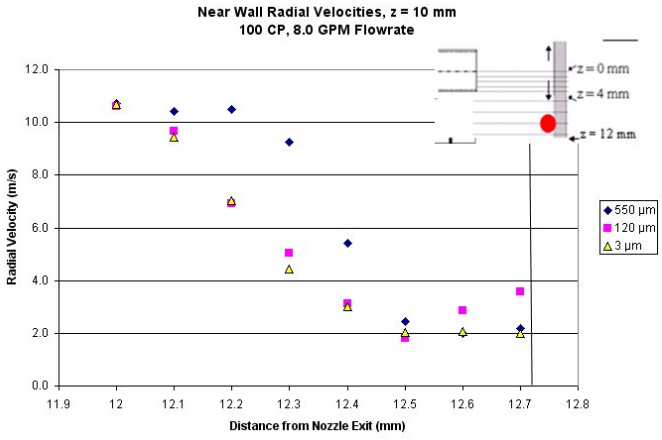

Figure 22: Near Wall Radial Velocities at z=10 mm for 100 CP Fluid

As opposed to the results at 3 mm from the centerline, Figure 22 clearly shows a variation in velocity

between the largest particles and the 120 and 3 micron particles. These largest particles appear to maintain a higher velocity when approaching the wall in the boundary layer region. As in previous results, a significant slip between the 120 and 3 micron particles is not evident. It is possible that the increased momentum of the 550 particles allows for these particles to better retain their initial velocity within a developed boundary layer located at an increased radial distance from the impinging jet. Experimental results from tests with less viscous fluids can provide additional insight to the overall effect of particle size in its tracking behavior.

4.2c Fluid Viscosity Constant at 1 CP - Effect of Particle Size in Turbulent Flow

The lowest viscosity case tested utilized pure water, which has a viscosity of 1 CP, as the carrier fluid. This low viscosity raised the Reynolds number for pipe flow through the nozzle to a value of about 85,000, which corresponds to fully turbulent flow. As for the other tests, three particle sizes of 550, 120, and 3 microns were seeded in the water in three separate experiments. Again, the fluid flow rate through the submerged nozzle was held constant at 8.0 gallons per minute, thus providing an average nozzle exit velocity of approximately 10.5 m/s. The measured axial velocity profiles at 1 mm from the nozzle exit are shown in Figure 23.

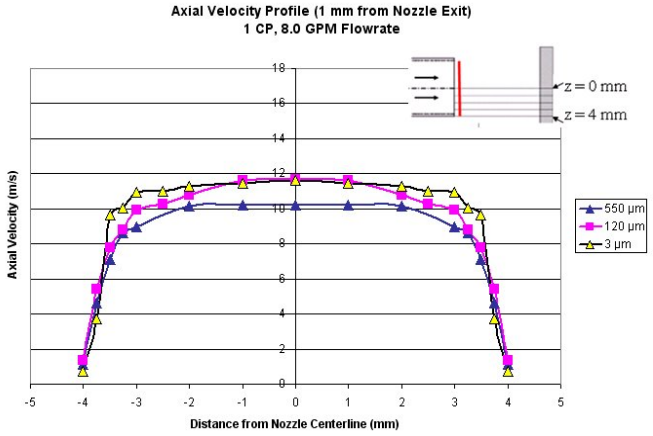

Figure 23: Axial Velocity Profile near Nozzle Exit for 1 CP Fluid

From these measurements with LDV, a turbulent velocity profile across the nozzle exit is evident. Axial velocities remain at a constant of about 10-12 m/s for the majority of the inner diameter region. These velocities sharply decrease to near-zero values at the nozzle wall, most likely due to shear stress at the nozzle wall. Again, velocity slip between the different particle sizes is seen in the near nozzle wall region, possibly from increased turbulence and wall interaction. Away from the nozzle walls, it appears that axial velocity decreases as particle size increases. This slip between the larger particles and the fluid may occur due to increased drag on the larger particles or direct interference with the wall inside the nozzle.

It is again of further importance to observe the axial velocities of the particles as they emerge from the submerged nozzle and travel toward the solid target. Figure 24 displays these axial velocities along the centerline of the nozzle. As in previous such plots, high initial axial velocities from the nozzle exit are noted, followed by a decrease at 8 mm from the exit. This decrease continues steadily until the particles reach the wall, with the final measurement location being 0.6 to 0.7 mm from the target. By this location, measured velocities are approximately 2 m/s.

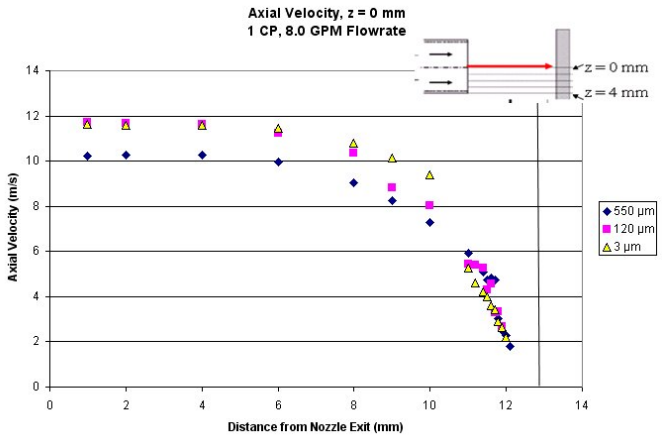

Figure 24: Axial Velocity versus Distance from Nozzle Exit at z=0 mm for 1 CP Fluid

Along this line of measurement, there appears to be some variation in the velocity values for the different sizes of particles tested. The 550 micron particles appear to consistently possess the lowest initial velocities, but follow a trend much like the two larger particle sizes, which results in minimal slip between the particles at the near target wall location. Once again, the decreased initial axial velocities for the largest particles may occur to increased drag and impact with the nozzle wall. Furthermore, it seems that the larger particles begin to decelerate at locations further from the target wall, which again may be caused by increased drag force acting on the larger particles. As mentioned, previously, however, all three particle sizes display similar velocities in the final 1-2 mm to the target, thus suggesting similar axial impact velocities at this location.

Figure 25 shows axial velocity plots at a line of measurement that is 3 mm from the nozzle centerline. Again, the largest particles appear to possess the lowest velocities at distances away from the target. Also, deceleration from the initial velocity recorded at the nozzle exit appears to occur sooner for the larger particles. Regardless of particle size, however, all axial velocities at the final measurement location prior to the target are approximately 2 m/s. It is also important to note that the slip in velocity for the different particle sizes appears to increase with distance from the nozzle centerline. These more noticeable variations in velocity may occur due to increased turbulence near to the nozzle wall or to direct contact of the larger particles with the wall.

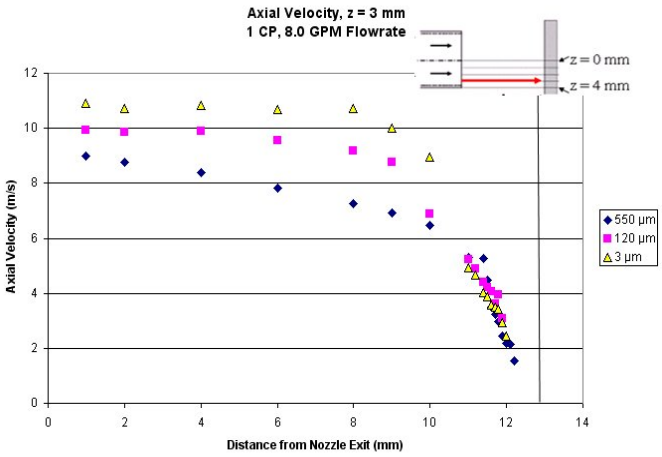

Figure 25: Axial Velocity versus Distance from Nozzle Exit at z=3 mm for 1 CP Fluid

As the seeded particles travel toward the target and away from the center of the nozzle, axial velocities decrease and ultimately become insignificant when compared to radial velocities. This velocity component, measured simultaneously with the axial velocities, describes flow in the direction parallel to the target. Figure 26 plots the measured particle radial velocities along a line of measurement which is 6 mm from the nozzle centerline. Note that along the nozzle centerline, or z=0 mm, radial velocities are near-zero as axial flow heavily dominates the flow in the center of the jet region.

As seen in this plot, initial radial velocities at the nozzle exit are nearly zero but begin to increase around 8 mm from the nozzle exit as flow begins to move outward in the radial direction. This increase in radial velocity results in a sharp peak within 1 mm from the target wall. In the final 1 mm to the wall, velocities largely maintain this peak value but experience some deviations which will be discussed in upcoming plots.

In general, it appears there is minimal slip in radial velocity between the largest and smallest particle sizes, especially in lines of measurement outside of the nozzle diameter. For most cases, an identical trend is observed for the different particle sizes as the rise in radial velocity occurs. There is some variation or slip in the peak and near-target wall region. Any slip in these locations may occur due to turbulence or interference from the target wall. The radial velocities in these near-wall regions are specifically addressed in upcoming plots and analysis.

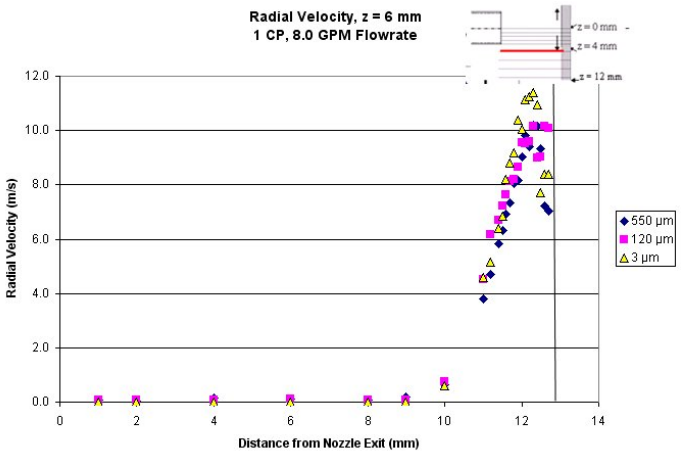

Figure 26: Radial Velocity versus Distance from Nozzle Exit at z=6 mm for 1 CP Fluid

Figure 27 displays the radial velocities recorded at 0.3 mm from the target wall for distances away from the nozzle centerline. As mentioned previously, this is the accurate measurement location nearest to the target. Furthermore, since axial velocities are less than 2 m/s along this line of measurement, especially for distances outside of the nozzle diameter, these values for radial velocity should provide an approximate impact speed of the particles at the target wall. As seen from the plot below, radial velocities surpass 6 m/s and reach maximum values around 4 to 8 mm from the nozzle centerline, where axial velocities are near-zero.

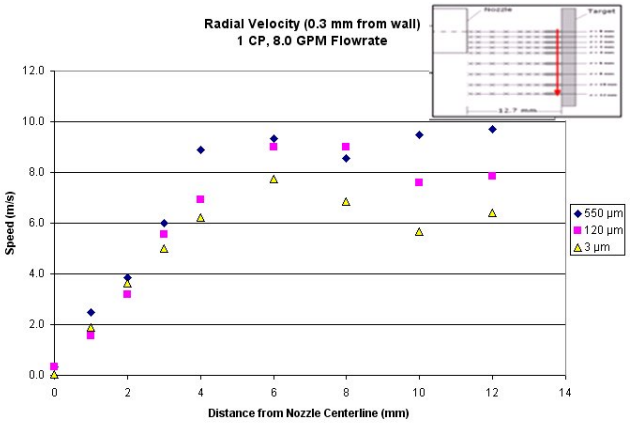

Figure 27: Radial Velocity versus Distance from Nozzle Centerline at 0.3 mm from Wall for 1 CP Fluid

It further appears that radial velocity increases with particle size, which is clearly seen for distances beyond 4 mm or the location of the nozzle wall. The larger particles seem to travel approximately 1-2 m/s faster than the carrier fluid, whose velocity is best approximated by the measurements made with the 3 micron particles. This slip may occur due to the increased momentum of the larger particles resulting from their increased mass. Once the initial axial momentum from

the jet is fully converted in the radial direction outside of 4 mm from the nozzle centerline, the larger particles can use their increased momentum to travel faster than the carrier fluid in the near-wall region. Since the carrier fluid has the lowest tested viscosity of 1 CP, it is expected that a much thinner and less visible boundary layer takes form along the wall.

In order to examine any change in radial velocity further away from the target, Figure 28 was constructed to plot the measured velocities at an additional 0.3 mm away from the target. Along this line of measurement, which is expected to be fully outside of any boundary layer or direct wall interference, radial velocity values appear to slightly increase when compared to the results of Figure 27. This increase is most significant for the smallest particles, which experience a maximum velocity of nearly 12 m/s at 0.6 mm from the wall and never exceed 8 m/s at 0.3 mm from the wall. Such a reduction may indicate a boundary layer formation between these two lines of measurement. At the same time, it should be noted that the more viscous fluids previously discussed experienced a more significant change in velocity between these two measurement locations.

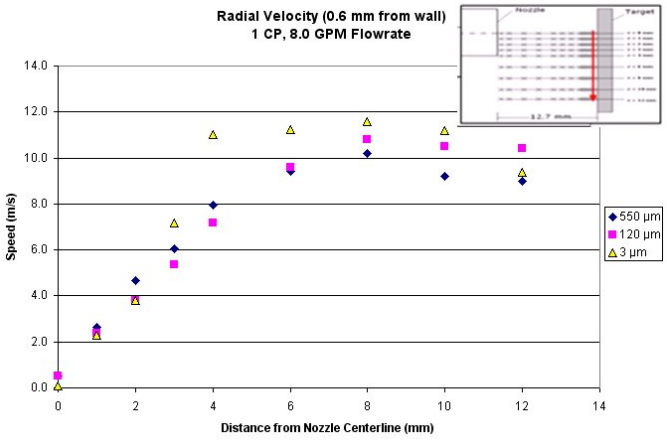

Figure 28: Radial Velocity versus Distance from Nozzle Centerline at 0.6 mm from Wall for 1 CP Fluid

As seen in the above results, there appears to be some slip in radial velocity between the different particle sizes, mainly at distances away from the nozzle wall. As opposed to the results at 0.3 mm from the wall, radial velocity appears to slightly decrease with increasing particle size. This slip or decrease may occur due to increased drag force acting on the larger particles as they travel away from the nozzle. Furthermore, it is important to note that although the radial velocity of the larger particles is generally lower at 0.6 mm from the wall, this velocity becomes higher than that of the carrier fluid at an additional 0.3 mm to the target. This may further demonstrate that despite possessing increased drag in the carrier fluid, the larger particles may carry the sufficient increased momentum to maintain higher impact speeds at the target.

It is also valuable to examine any near-wall change in radial velocity inside and outside of the nozzle diameter. Figure 29 displays measured radial velocities in this near wall region along 3 mm from the nozzle centerline. Again, note that the two final measurements at 12.6 and 12.7 mm from the nozzle exit lack the accuracy of the other measurement locations. With this being the case, it is important to consider 12.5 mm from the nozzle exit, or 0.3 mm from the target wall, the final accurate LDV radial velocity measurement prior to particle impact.

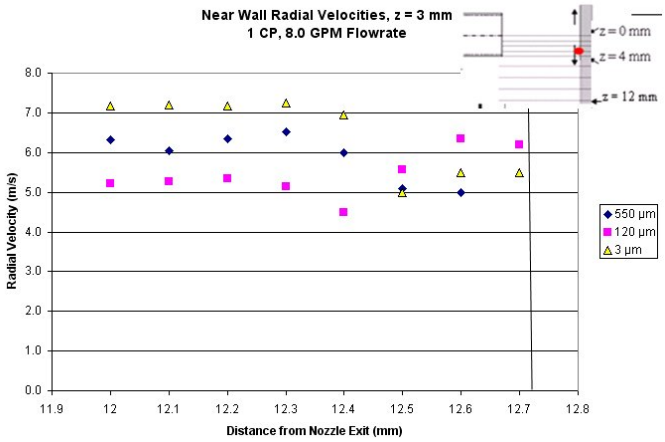

Figure 29: Near Wall Radial Velocities at z=3 mm for 1 CP Fluid

It is evident from the plot above that a significant change in radial velocity does not take place for the larger particles in this near-wall region. The 3 micron particles, however, which best follow the carrier fluid, possess a slight drop in velocity at 0.3 mm from the target. As mentioned earlier, this may signify the beginning of a thin boundary layer along the target. Since the larger particles have increased momentum, it is likely they penetrate the boundary layer region and maintain higher velocities despite having reduced velocities away from the wall.

Figure 30 seen below plots near wall radial velocities at 10 mm from the nozzle centerline, or at a location where flow in the radial direction should be more developed. Again, the smallest particles experience some reduction in velocity at 0.3 mm from the target. At the same time, the 550 and 120 micron particles again display much less reduction in velocity. As noted earlier, the increased momentum of the larger particles coupled with the thin boundary layer formed by the 1 CP fluid may prevent any reduction in the velocity of the larger particles at the target wall.

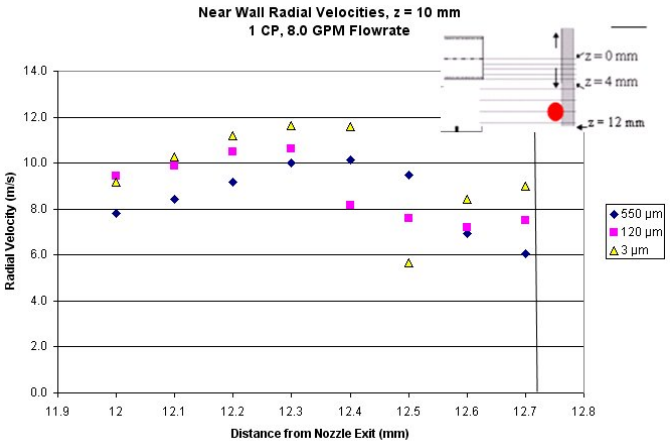

Figure 30: Near Wall Radial Velocities at z=10 mm for 1 CP Fluid

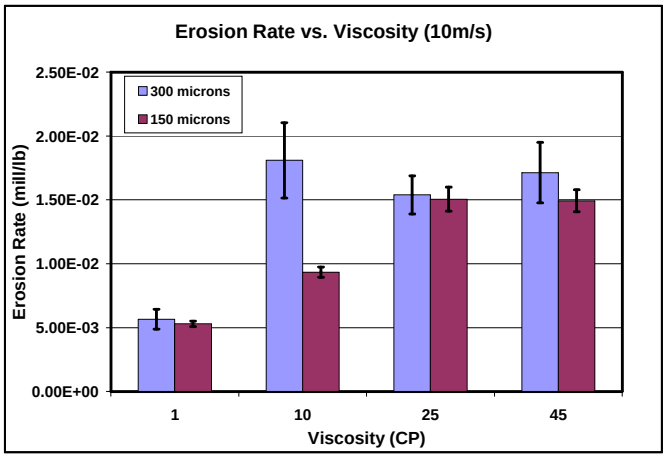

Figure 31: Erosion Rate for 300 and 150 µm Particles for Different Fluid Viscosities

The effect of the carrier fluid's viscosity and seeded particle's size on its tracking has been presented by way of axial and radial velocity measurements using LDV. Erosion measurements for similar fluid viscosities and particle sizes will aid in displaying the effect of these variables on a target wall's metal loss or erosion rate.

5. EXPERIMENTAL EROSION DATA

5.1a ER Probe Results -- Erosion Rate versus Viscosity

Erosion measurements were made using an Electrical-Resistance (ER) probe for the same direct impingement geometry studied with LDV. The submerged nozzle maintained a constant flow rate of 8.0 gallons per minute, thus producing an average velocity of about 10 m/s through the exit. Again, note that the flat probe surface was placed 12.7 mm away from the 8 mm diameter nozzle. The carrier fluid viscosity was varied between 1, 10, 25, and 45 CP using appropriate amounts of CMC, or carboxyl methyl cellulose, dissolved in water. Oklahoma #1 sand having an average size of 150 microns or California 60 with an average sand size of 300 microns was added to the fluid. Sand concentrations through the nozzle exit were measured manually while the metal loss rate over time was recorded by way of an ER probe. The erosion rate was then found in terms of target wall loss in mils per pound of sand traveling through the nozzle exit. Figure 31 below shows the measured erosion rate for the four tested fluid viscosities when using the 150 and 300 micron sands. Average erosion rates along with uncertainty ranges are shown and are based on repeated experiments performed by Okita in 2008.

As seen from the above results, the erosion rate appears to increase when viscosity is raised from 1 to 10 CP and when either particle size is used. This increase is more significant when the larger 300 micron sand particles are submerged in the fluid. When viscosity increases from 10 to 25 CP, the erosion rate experiences a notable increase when the smaller 150 micron sand is used, while the erosion measurement stays approximately constant with the larger sand size. The erosion rate appears to remain constant for both sand sizes when the carrier fluid viscosity is raised further from 25 to 45 CP. For nearly all viscosity cases, the 300 micron sand produces a slightly higher measured erosion rate than the smaller 150 micron sand. When the carrier fluid viscosity was maintained at 10 CP, the 300 micron CA 60 sand resulted in an erosion rate nearly twice as high as the 150 micron OK #1 sand. While an increase in erosion rate from larger sand size may be explained by the increased mass and momentum of the larger impinging particles, the effect of viscosity on the measured erosion rate must be examined further.

Since the carrier fluids used in the erosion measurements were obtained with CMC and water, a mixture which may be non-Newtonian at higher viscosities, certain ER probe experiments were repeated using water and glycerin mixtures, which are known to display fully Newtonian behavior and were used in LDV experiments. Figure 32 below displays the measured erosion rates for the 300 micron sand in carrier fluid viscosities created from CMC-water and glycerin-water mixtures. Again, average erosion rates along with uncertainty ranges are shown and are based on repeated experiments performed by Okita in 2008.

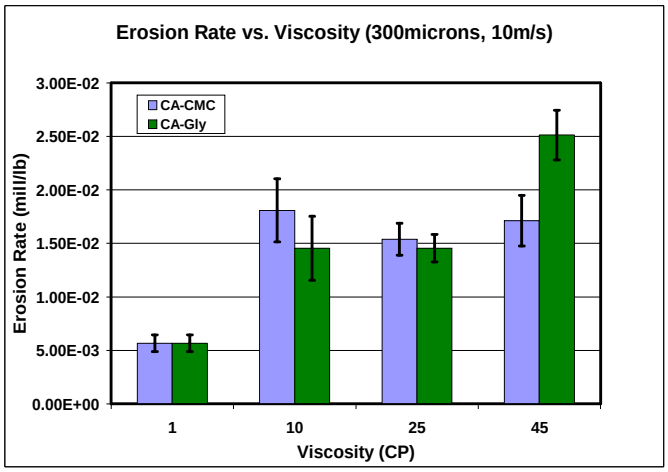

Figure 32: Erosion Rate for 300 µm Particles using CMC and Glycerin to Change Fluid Viscosity

As seen from Figure 32, CMC-water and glycerin-water mixtures produce approximately the same erosion rate measurements when lower viscosities of 1, 10, and 25 CP are used. At the highest viscosity of 45 CP, there is a more significant discrepancy in the erosion rate measurements of the two different mixtures. It is possible that above 25 CP, the CMC-water mixture is less Newtonian and may create an additional impact on measurements in more viscous fluids. Nevertheless, the effect of sand particle size and carrier fluid composition on the measured erosion rate has been demonstrated by way of these measurements. The values obtained from ER probe testing can further be related to near-wall particle velocity measurements obtained previously from LDV experiments.

5.1.b Comparison of Erosion Results to LDV Measurements

The plot seen on the following page in Figure 33 displays the average radial velocity at 0.3 mm from the target wall obtained from LDV measurements and average erosion rate recorded from ER probe measurements, with both types of data plotted as a function of carrier fluid viscosity. An average radial velocity value was obtained by finding the mean of all the LDV measurements at 0.3 mm from the wall. In other words, the average is based on the line of measurement which is located 0.3 mm from the target and extends from the nozzle centerline in a radial direction outward to z=12 mm. This velocity value is the best estimate for average particle impact speed at the target, since it is based on the final accurate and nearest-wall LDV measurements. At the same time, it is known that axial velocity is small and relatively insignificant in this region.

It is important to note that the two different types of measurements compared in Figure 33 are largely a sole function of fluid viscosity. Aluminum particles used in LDV measurements have an average size of 120 microns, while the sand particles in the erosion rate experiments possess a comparable size of 150 microns. Furthermore, for both types of tests, carrier fluid viscosities were maintained at approximately 1, 10, 25, and 50 CP. The highest viscosity case of 100 CP was not used in erosion rate measurements and is thus not shown in Figure 5-3. Finally, it was seen in Figure 32 that the CMC-water mixture displayed largely Newtonian behavior, much like the glycerin-water concoction used in particle velocity measurements. Overall, it is seen that discrepancies in particle size, viscosity, and fluid mixture type are minimized. Consequently, the velocity and erosion rate results seen on the following page are controlled mainly by a change in fluid viscosity.

As seen in Figure 33, the average radial velocity at 0.3 mm from the target wall appears to decrease with increasing viscosity. At the same, the measured erosion rate, in mils of wall loss per pound of sand through the nozzle exit, increases with increasing viscosity. In general, there appears to be an inverse relationship between average radial velocity at 0.3 mm from the target and the measured erosion rate. While the average velocity at 25 CP is approximately one-third of the velocity measured at 1 CP, the erosion rate at 25 CP is about three times higher than the measurement at 1 CP. Above fluid viscosities of 25 CP, both erosion rate and average radial velocity remain approximately constant.

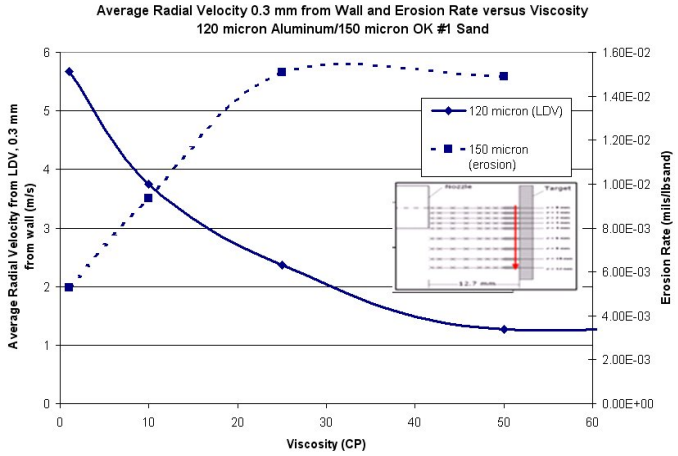

Figure 33: Average Radial Velocity 0.3 mm from Wall and Erosion Rate versus Viscosity

The results above indicate a contradiction in that decreased particle velocity at a distance very near to the wall results in an increased erosion rate. It is possible that the ER probe used to make erosion rate measurements lacks the flat surface of the target used in LDV measurements, thus inducing increased near-wall turbulence which may prevent the formation of a boundary layer seen in previous discussion. Furthermore, if post-impact velocities with the target are actually being recorded at 0.3 mm from the target, then the trend seen in Figure 33 is more likely since a decreased post-impact velocity would correspond to larger momentum transfer from the particle to the wall. It is also possible that erosion is mainly dictated by the largest particle sizes seen in the sand distribution. If this were the case, then the larger particles would possess impact velocities more similar to that

of the smaller particles outside of a boundary layer. Thus, it is possible that erosion correlates better with the velocity trend of particles outside of a developed boundary layer.

Figure 34 below displays the average radial velocity at an additional 0.3 mm from the wall, or 0.6 mm total away from the target. The erosion rate caused by OK #1 sand, which has an average size of 150 microns, is also shown again. This plot is constructed like that of Figure 5-3 and incorporates data from the same experiments. Since the velocity measurements are at a distance of 0.6 mm from the wall, particles traveling in this region possess higher average radial velocities as they have yet to enter a boundary layer.

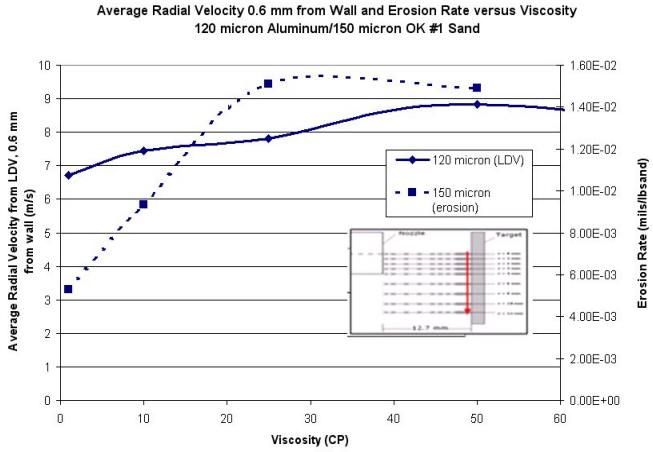

Figure 34: Average Radial Velocity 0.6 mm from Wall and Erosion Rate versus Viscosity

It is evident from the results above that a slight increase in average radial velocity across the face of the target is observed as the carrier fluid viscosity increases. Most likely, this occurs due to increased particle radial velocities away from the boundary layer resulting directly from higher nozzle exit axial velocities. Recall from previous discussion that as viscosity increased, the maximum axial velocity across the nozzle exit also increased as a transition from turbulent to laminar flow took place inside the nozzle. As mentioned earlier, it is possible that the largest particles in the OK #1 sand size distribution retained these increased velocities until the particles impacted the target. In other words, the high momentum of the larger particles prevented a significant decrease in velocity at the target caused by the boundary layer. This may partly explain the measured increase in erosion rate as fluid viscosity was raised.

6. SUMMARY AND CONCLUSIONS

Fluid and particle velocity measurements using Laser Doppler Velocimetry (LDV) were obtained for direct impingement jet flow using various liquid viscosities and particle sizes. Axial and radial velocity components were recorded for aluminum particles with an average size of 3, 120, and 550 μm in a liquid with a viscosity ranging from 1 to 100 CP. Impact velocities were obtained for locations as near as 0.2 to 0.3 mm from the target surface.

LDV measurements indicated a transition from turbulent to laminar flow as viscosity was increased. Velocity slip between the fluid and larger particles was minimal at the nozzle exit, namely for the more viscous fluids. Along the target surface, radial velocity measurements showed a boundary increasing in thickness with increased viscosity. Particle velocities decreased with increasing viscosity within the observed boundary layer, while velocities increased with increasing viscosity just outside of this wall shear region. Furthermore, larger particles possessed higher velocities inside the boundary layer along the target, despite having slightly lower radial velocities outside of this near-wall region. Additional slip between the fluid and particle was seen to be minimal away from the wall.

Erosion rate measurements were made with Okita (2008) using an Electrical-Resistance (ER) probe for an identical geometry with fluid viscosities ranging from 1 to 45 CP and average sand particle sizes of 150 μm and 300 μm. Preliminary results displayed an increase in erosion rate with increasing viscosity. Since the average measured particle impact velocity decreased with increasing viscosity, it is possible that larger particles in the sand size distribution penetrated the observed boundary layer and impacted the ER probe. At the same time, an uneven probe surface may have increased turbulence at the eroding target, thus negating the effect of increased boundary layer thickness with increased viscosity.

6.1 Recommended Future Work

Additional studies need to be performed to better assess the surface of the ER probe in order to ensure that the erosion target is as flat or even as the target used in LDV testing. Furthermore, similar LDV and ER probe experiments must be performed to determine a more accurate value of uncertainty in particle velocity and erosion rate measurements. At the same time, further analysis of turbulent intensities and velocity fluctuations will aid in better estimating such uncertainty values for LDV results. Finally, Computational Fluid Dynamics (CFD) results for particle tracking and erosion rate must be validated by direct comparison of such experimental findings.

Future LDV testing should also include the adjustment of the experimental apparatus and testing tank to ensure velocity measurements can be obtained closer than 0.3 mm from the wall. The amount of bubble entrainment in the carrier fluid should be further reduced, especially for viscosities of 10 and 25 CP. It may also be of value to vary the fluid flow rate through nozzle in order to change the average exit velocity and observe the effect on particle tracking.

7. REFERENCES

[1] H.S. Meng, K.C. Ludema, Wear models and predictive equations: their form and content, Wear 181-183 (1995) 443-457.

[2] J.G.A. Bitter, A study of erosion phenomena, parts I, II, Wear 6 (1963) 5-21,169-190.
[3] H.M. Clark, The influence of the flow field in slurry erosion, Wear 152 (1992) 223-240.
[4] H.M. Clark, On the impact rate and impact energy of particles in a slurry pot erosion tester, Wear 147 (1991) 165-183.
[5] K.K. Wong, H.M. Clark, A Model of particle velocities and trajectories in a slurry pot erosion tester, Wear 160 (1993) 95-104.
[6] J.M.M. Barata, D.F.G. Durao, Laser-doppler measurements of impinging jet flows through a crossflow, Experiments in Fluids 36 (2004) 665-674.
[7] O. Sasaki, T. Abe, T. Shimizu, Simultaneous measurement of falling velocity and size of large droplets using a laser system, Applied Optics, 19-7 (1989) 1151-1153.
[8] R. Ancimer, J. Wallace, H. Jaaskelainen, Investigations into the effect of LDV seed particles on the operating characteristics of a spark ignition engine, Experiments in Fluids 27 (1999) 175-180.